



An integrated analysis of the fecal metabolome and metagenome reveals the distinct effects of differentially charged nanoplastics on the gut microbiota-associated metabolites in mice

Miaomiao Teng ^a, Xiaoli Zhao ^{a,*}, Lingfeng Zhou ^a, Hong Yan ^b, Lihui Zhao ^a, Jiaqi Sun ^c, Yunxia Li ^c, Wentao Zhu ^d, Fengchang Wu ^{a,*}

^a State Key Laboratory of Environmental Criteria and Risk Assessment, Chinese Research Academy of Environmental Sciences, Beijing 100012, China

^b Department of Environmental Health Sciences, Yale School of Public Health, Yale University, USA

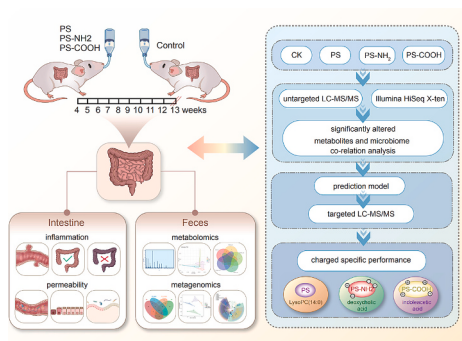
^c School of Energy and Environmental Engineering, University of Science and Technology Beijing, Beijing 100083, China

^d Innovation Center of Pesticide Research, Department of Applied Chemistry, College of Science, China Agricultural University, Beijing 100193, China

HIGHLIGHTS

- Differentially charged PS-NPs cause intestinal impairments in mice.
- Fecal metabolites and gut microbiome were altered by differentially charged PS-NPs.
- Potential biomarkers using model caused by nanoplastics in a charge-specific manner.
- The biomarkers enable a thorough evaluation of the health effects of PS-NPs.

GRAPHICAL ABSTRACT



ARTICLE INFO

Editor: Anastasia Paschalidou

Keywords:
Differential charges
Nanoplastics
Gut microbiome
Metabolomics
Mice

ABSTRACT

Whether nanoplastics with differential charges cause intestinal impairment via distinct mechanisms remains unclear. We investigated the relationship between fecal metabolites and the gut microbiome, and potential biomarkers thereof, in mice following exposure to differentially charged polystyrene nanoplastics (PS-NPs). Metagenomic analysis revealed that exposure to differentially charged PS-NPs resulted in alterations in the abundances of *Bilophila wadsworthia*, *Helicobacter apodenus*, and *Helicobacter typhlonius*. A total of 237 fecal metabolites were significantly altered in mice that exhibited intestinal impairment, and these included 10 gut microbiota-related fecal metabolites that accurately discriminated impaired intestinal samples from the control. Additionally, the specific gut microbiome-related fecal metabolite-based model approach for the prediction of intestinal impairment in mice had an area under the curve (AUC) of 1.0 in the PS (without charge) group, an AUC of 0.94 in the PS-NH₂ (positive charge) group, and an AUC of 0.86 in the PS-COOH (negative charge) group. Thus, the model showed promising evaluable accuracy for the prediction of intestinal impairment induced by

* Corresponding authors at: State Key Laboratory of Environmental Criteria and Risk Assessment, Chinese Research Academy of Environmental Sciences, Anwai Dayang Fang 8#, Chaoyang District, 100012 Beijing, China.

E-mail addresses: zhaoxiaoli_zxl@126.com (X. Zhao), wufengchang@vip.skleg.cn (F. Wu).

nanoplastics in a charge-specific manner. Our study demonstrates that the fecal metabolome of mice with intestinal impairment following exposure to differentially charged nanoplastics is associated with changes in the gut microbiome. The identified biomarkers have potential application for the detection of intestinal impairment after exposure to negative, positive, or noncharged nanomaterials.

1. Introduction

Due to their unique economic application value, convenience, and light weight, plastics play important roles in daily human life, and the fight against COVID-19 has led to increased usage of plastics (Gao et al., 2022). To combat the global plastic pollution crisis, the United Nations Environment Assembly (UNEA) created an international legal agreement (Simon et al., 2021). However, plastics are usually fragmented into microplastics (MPs, <5 mm) and nanoplastics (NPs, 1–100 nm), which have been detected in aquatic environments, air, soil, food, and containers, thus posing a relatively severe, ubiquitous threat. The lung tissue, serum, and feces of adults and infants have been shown to contain MPs/NPs (Jenner et al., 2022; Leslie et al., 2022; Yan et al., 2022; Zhang et al., 2021). However, the concentrations of NPs in natural aquatic environments have been found to be lower than 1 mg/L (Lenz et al., 2016). NPs have become an increasingly pressing challenge in the worldwide, and their early identification is recognized as an effective approach to reduce the health risk they pose to organisms. The underlying health risk of NPs also needs to be investigated to reduce their toxicity.

In natural environments, pristine plastics degrade to weathered MPs or NPs under UV irradiation, biodegradation, physical abrasion, chemical oxidation, and heat irradiation (Luo et al., 2022). In addition, the salinity, pH, and dissolved organic molecules in aquatic environments significantly alter the physicochemical properties of MPs and NPs. The multiple aging processes that plastics undergo damage the chemical bonds of their polymers and lead to the formation of new functional groups. These functional groups may change the surface charges of MPs and NPs (Li et al., 2022), and many surface charges on NPs in turn affect their environmental fate, behaviors, and effects. The anionic COOH-group and the cationic NH₂-group are commonly detected on the surfaces of NPs in the environment (Casado et al., 2012; Chen et al., 2023a). Several investigations have focused on the toxic effects of differently charged NPs in aquatic organisms. For example, polystyrene (PS)-COOH were reported to induce a more severe lethal effect on *Daphnia magna* than PS-NH₂ (Wei et al., 2019). In contrast, the exposure of sea urchin embryos to 2.5–10 mg/L PS-NH₂ was found to inhibit their development and induces malformation, whereas exposure to up to 50 mg/L PS-COOH had little impact on embryo development (C. et al., 2014). The acute toxicity of PS-NH₂ in zebrafish embryos/larvae is distinct from that of PS-COOH. Positively and negatively charged PS-NPs inhibit the locomotor behaviors of zebrafish differently due to their combination with different neurotransmitter receptors (Teng et al., 2022b). The accumulation of NPs in the small intestines, large intestines, brains, testes, and spleens of mice were observed after oral exposure to 100 nm PS, PS-NH₂, PS-COOH (100 μL 10 mg/mL) (Xu et al., 2021). Oral gavage of 70 nm and 5 μm PS, PS-NH₂, and PS-COOH MPs/NPs in mice for 28 days induced gut barrier dysfunction and decreased the expression of tight junction proteins (Qiao et al., 2021). An in vitro assay revealed that 10 mg/L of 80 nm PS-COOH and PS-NH₂ activated the ROS-MAPK/NF-KB signaling pathways and induced inflammation and cytotoxicity in the macrophage cell line Raw 264.7 (Chen et al., 2023b). PS-NH₂ and PS-COOH easily entered into the intestinal epithelial Caco-2 cells, thus disrupting the tight junctions between cells (Xu et al., 2021). These findings indicate that the different toxic effects of NPs on organisms are regulated via a complex process that is dependent on not only the type of NPs but also the differential charges of NPs.

The recently increased global concerns regarding NPs highlight the need to expand the efforts to improve the health of organisms. The

intestine is known as a crucial line of defense against invasion by harmful chemicals or environmental factors and prevents exogenous and endogenous molecules from metastasizing in the intestinal tract to enter the systemic circulation (Agirman et al., 2021). Importantly, the compositions and functions of the gut microbiome contribute to the maintenance of intestinal epithelial access, the absorption and digestion of nutrients, and the integrity of the intestinal barrier (Desai et al., 2016; Rakoff-Nahoum et al., 2016). Notably, an increasing number of studies have revealed changes in the intestinal microbiome of NP-exposed organisms (Jacob et al., 2020; Santos et al., 2022). Due to their small size, large surface area, and high mobility, NPs can cross the gastrointestinal barriers of organisms, block the digestive tract and remain in the body for long periods, thereby affecting the gut microbiota homeostasis (Santos et al., 2022). Additionally, the changes in the gut microbiome in organisms after NPs exposure are attracting increasing attention. The gut microbiota composition can be markedly altered in organisms exposed to NPs. The severity of intestinal damage and changes in the microbiota composition can be measured by pathological examination and DNA sequencing tools, respectively.

Several studies have demonstrated that the gut, which is considered the second brain, exerts a profound effect on immunity and metabolism (Fan and Pedersen, 2021; Garrett, 2020). Importantly, the occurrence of gastrointestinal diseases is associated with alterations in the immune response and metabolic profiles (Maloy and Powrie, 2011; Raskov et al., 2016). Metabolomics mainly studies the changes in endogenous metabolites associated with biological processes induced by external stimuli and pathophysiological changes and can more directly and accurately reflect the physiological state of organisms (Han et al., 2021). The gut microbiota encodes various of metabolic pathways in the host. Gut microorganisms produce numerous compounds that influence the health of the host (Han et al., 2021). These microbiota-driven metabolites affect cognition, behaviors, metabolism, immune functions, obesity, carcinogenesis and cardiovascular health (Cani, 2019; Lynch and Hsiao, 2019; Rooks and Garrett, 2016; Sonnenburg and Bäckhed, 2016). The combination of metabolomic profiling and metagenome analysis is increasingly recognized as an efficient approach for the detection of adverse effects after exposure to various environmental contaminants (Coryell et al., 2018; Li et al., 2019; Lindell et al., 2022). However, crucial data on the specific effects of charged/noncharged PS-NPs on mammals, particularly on mammalian gastrointestinal diseases, revealed by studying the fecal metabolome and metagenome are limited.

The gut microbiota-derived metabolites in fecal samples are influenced by environmental contaminants or pathological conditions (Lin et al., 2021). A literature review revealed that no study has investigated whether the intestinal impairment induced by MP or NPs with different charges could be differentiated from a control group exposed to non-charged MPs/NPs based on specific differential metabolites in fecal samples.

In this study, we exposed mice to differentially charged NPs and performed histopathological examination and gene expression analysis for the assessment of intestinal damage, utilized metagenomic approaches to analyze the gut microbiome in cecal contents, and used LC-MS/MS-based metabolomics tools to identify the potentially affected biological pathways in fecal samples. We also identified a promising charge-specific biomarker panel comprising gut microbiota-derived metabolites involved in intestinal inflammatory responses in male mice following exposure to differentially charged PS-NPs. These data may provide adequate information on the health risks associated with,

and shed light on the potential mechanisms and metabolic biomarkers of exposure to PS-NPs with different charges.

2. Materials and methods

2.1. Chemicals

Forty-four nanometer nonfunctionalized PS-NPs, 51 nm PS-NH₂ and 50 nm PS-COOH, as 10 % stock solutions, were purchased from Bangs Laboratories, Inc. (Fishers, IN, USA). All NPs were diluted with Milli-Q water to 20 g/L for storage. All other chemicals were of chromatographic grade.

2.2. Animal husbandry and sample preparation

Wild-type male ICR mice (4 weeks old, 29.2 ± 0.30 g) were purchased from Beijing Vital River Laboratory Animal Technology Co., Ltd., and bred in the China Agricultural University Laboratory Animal Facility. All mice were group housed in ventilated and sterilized cages under a 12 h light/12 h dark cycle, a temperature of 22 ± 2 °C, and 40–60 % relative humidity. All mice were fed a 5053 PicoLab Rodent Diet (LadDiet). After two weeks of acclimation, the mice were randomly assigned to four groups (vehicle (CK), 80 µg/L PS, 80 µg/L PS-NH₂, and 80 µg/L PS-COOH, n = 6 mice per group), and it was ensured that there was no significant difference in the average body weight between the groups at the beginning of the experiment. The concentrations of NPs (80 µg/L) used in this study were markedly lower than the observed-effect concentrations (>1 mg/L) in previous studies (Al-Sid-Cheikh et al., 2018; Xiao et al., 2022). In addition, in mammals, the pathways of exposure to NPs are more complex and diverse; thus, we selected the concentration of 80 µg/L from the range of environmentally relevant concentrations (0.1–100 µg/L) (Lenz et al., 2016; Xiao et al., 2022). MPs/NPs have been frequently detected in water bodies. Therefore, it is possible that NPs present in drinking water penetrate into tissues and accumulate in human organs. In addition, to avoid the confounding effects of chronic stress induced by oral gavage, the NPs were administered in the drinking water ad libitum. The unexposed (CK) mice received drinking water containing 0.01 % v/v SDS as control. The drinking water was prepared and changed twice a week. After 9 weeks of exposure, all male mice were fasted for 4 h and sacrificed. Their colon and cecal contents were collected, frozen immediately in liquid nitrogen and stored at -80 °C until further analysis. All animal husbandry and experiments were performed with approval from the China Agricultural University Animal Care and Ethical Committee (No. AW30302202-5-1).

2.3. Collection of intestinal samples for histology

Samples of parts of the colons from three male mice randomly selected from each group were fixed in 4 % formaldehyde for histological examination. After 24 h of fixation, the colon samples were cut into 5 µm thick sections, embedded in paraffin, stained with hematoxylin and eosin (H&E) or Alcian blue-periodic acid-Schiff (AB-PAS) and then analyzed using Olympus microscope (Olympus Corp., Tokyo, Japan) and ImageJ Pro software.

2.4. Quantitative reverse transcription polymerase chain reaction (qRT-PCR)

Total RNA was extracted from the colon samples (20–25 mg) based on the manufacturer's instructions (TRIzol reagent; Tiangen Biotech CO., LTD., Beijing, China). The RNA quality and concentration were measured using a NanoDrop (ThermoFisher Scientific Inc., Waltham, MA, USA.). RNA (2 µg) from each sample was converted to cDNA using the First-cDNA synthesis kit (Tiangen, Beijing, China). Gene expression in the intestine was measured using SYBR Green PCR master mix (Tiangen, China) and analyzed using an ABI 7500 Fast Real-Time PCR

system (ThermoFisher Scientific) as previously described (Teng et al., 2022c). The expression levels of the target genes were normalized to the Gapdh mRNA level in each sample, calculated with the 2^{-ΔΔCt} method, and are presented as the fold changes relative to the CK group. The primer sequences were obtained from Sangon Biotechnology (Shanghai, China) (Teng et al., 2022a).

2.5. Shotgun metagenomic analysis

Frozen mouse cecal contents were stored at -80 °C for shotgun metagenomic analysis (n = 3 replicates). Microbial DNA extraction was performed using a commercial DNeasy PowerSoil kit (QIAGEN, Inc., Netherlands) according to the manufacturer's instructions. The quality and quantity of total microbial genomic DNA samples were measured using agarose gel electrophoresis and with a NanoDrop ND-1000 spectrophotometer (Thermo Fisher Scientific Inc., Waltham, MA, USA). The extracted DNA was used to construct metagenome shotgun sequencing libraries with insert sizes of 400 bp using an Illumina TruSeq Nano DNA LT Library Preparation Kit (Illumina, San Diego, CA, USA). Each library was sequenced using the Illumina HiSeq X-ten platform with the PE150 strategy. Whole-genome sequencing was performed to analyze the taxonomic and functional profiles of the gut microbiome (Huang et al., 2019). Further details of the method used for shotgun metagenome analysis are included in Text S1.

2.6. Untargeted metabolomic profiling

Fecal samples from the cecum were used for untargeted metabolomics analysis. Briefly, approximately 50 mg of fecal samples (-80 °C) were used for untargeted metabolomics analysis, and five to six replicates of each treatment were prepared. A precooled mixture (methanol: acetonitrile:water = 2:2:2, v/v) was added to the sample tube, which was then vortexed for 1 min, sonicated for 30 min in an ice-water bath, incubated for 10 min at -20 °C, and homogenized at 14,000 ×g for 20 min at 4 °C. The supernatant was dried under vacuum, redissolved in 100 µL solvent (acetonitrile: water = 1:1, v/v), vortexed, and homogenized at 14,000 ×g for 15 min at 4 °C. Eighty microliters of supernatant were then used for subsequent analysis. Untargeted metabolites were quantified by Agilent 1290 Infinity liquid chromatography-AB Triple TOF 6600 mass spectrometry (LC-MS/MS). Further details of the methods used for untargeted metabolomics analysis are included in Text S2.

2.7. Targeted metabolomic profiling

The levels of 1-myristoyl-sn-glycero-3-phosphocholine, deoxycholic acid, and indoleacetic acid in the samples were quantified by liquid chromatography (LC20A) coupled with 5500 QTRAP mass spectrometry (AB SCIEX) in the positive ion mode. A Waters UPLC BEH Amide column (1.7 µm, 2.1 × 100 mm column) was used for chromatographic separation. Details of the extraction methods and instruments are provided in Supplementary Table S1.

2.8. Statistical analysis

Data preprocessing, statistical analysis, predictive model building, and fecal microbiome-metabolomics correlation analysis were performed using R programming (V.4.1.3). Principal coordinate analysis (PCoA) of metagenomics using Bray-Curtis distance matrices was performed using the QIIME software to estimate beta diversity. For metabolomics data processing, we used quantile normalization, log-transformation, and Pareto scaling. Principal component analysis (PCA) of metabolomics was visualized to identify the initial trends in datasets. Metabolites with an adjusted *P* < 0.05 determined by Student's *t*-test and a variable importance value (VIP) > 1 were considered as significantly altered. The statistical analysis of certain metabolites and

gut microbiome species was conducted using SPSS (version 16.0.1; USA). Receiver-operating characteristic (ROC) analysis was performed using the GraphPad Prism software (San Diego, CA, USA) to assess the sensitivity, area under the ROC curve (AUC), and specificity of specific metabolites in the metabolomics data of the groups of differentially charged PS-NPs. All results are expressed as the mean \pm standard deviation (S.D.). Differences in other parameters with $P < 0.05$ determined by one-way ANOVA with Tukey's HSD multiple comparison post-test were considered significant.

3. Results

The results from the histopathological analysis of the mouse colon are shown in Fig. 1A–C. H&E staining of colon sections revealed

increased inflammatory cell infiltration after exposure to PS with different charges (Fig. 1A). The histological scores of the colon were significantly increased (Fig. 1B) after exposure to PS, PS-NH₂, and PS-COOH. AB-PAS-stained sections revealed the presence of mucin, but no significant difference in the ratio of goblet cells were detected (Fig. 1A, C).

Differentially charged PS-NPs changed the expression of genes related to intestinal inflammation and permeability (Fig. 1D). They induced an immune response in the colon, indicated by a strong tendency toward downregulated expression of the *interferon-γ (IFNγ)*, *trefoil factor-3 (Tff-3)*, *interleukin-1b (IL-1b)*, *interleukin-6 (IL-6)*, and *interleukin-10 (IL-10)* genes. In addition, the expression of *IL-1b* was significantly downregulated after exposure to positively and negatively charged PS-NPs compared to the noncharged PS-NPs. We also found a

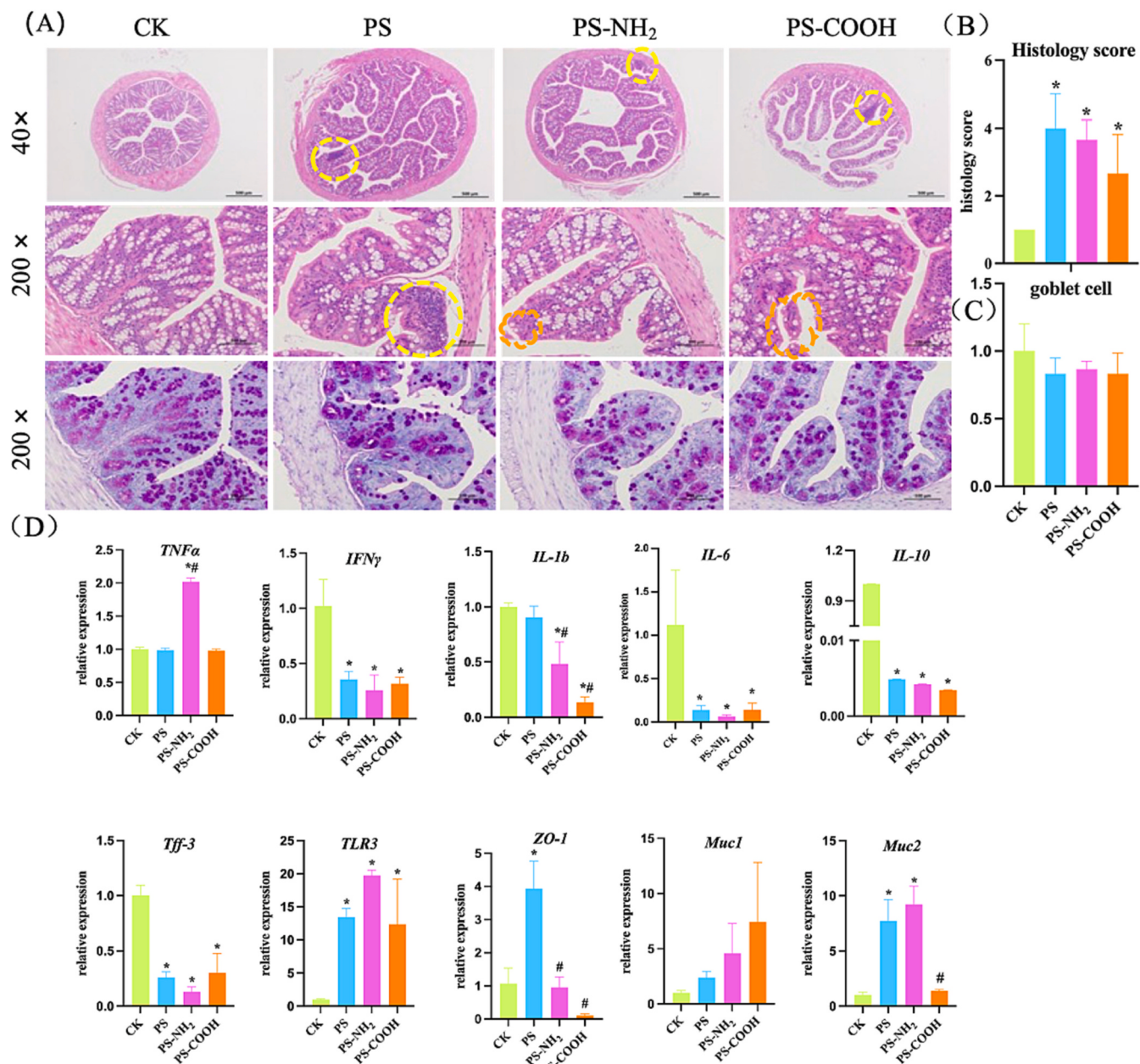


Fig. 1. Effects of exposure to differentially charged PS-NPs on the histopathology and inflammatory responses in mice ($n = 5$ –6 replicates). A. Representative images of histopathological alterations in the mouse colon after exposure to PS, PS-NH₂, and PS-COOH (40 \times , 100 \times , 200 \times). The yellow circle indicates inflammatory cell infiltration, and the orange circle indicates intestinal epithelial cell abscission. B. Histological score of the colon. C. Fold change of goblet cells in the colon. D. qRT-PCR was used to measure the relative expression of *TNFα*, *IFNγ*, *IL-1b*, *IL-6*, *IL-10*, *Tff-3*, *TLR3*, *ZO-1*, *Muc1*, and *Muc2* in the colon samples. The data are expressed as the mean \pm S.D. * $P < 0.05$ vs. the control group (CK), and # $P < 0.05$ vs. the PS group.

significant upregulation of *mucosa 2* (*Muc2*) and *Toll-like receptor-3* (*TLR-3*) gene expression in mice treated with differentially charged PS compared with CK mice. Exposure to PS-NH₂ treatment also increased metabolic inflammation in the colon, as indicated by an elevated circulating level of *tumor necrosis factor α* (*TNFα*) mRNA. The expression of *mucosal 1* (*Muc1*) gene did not differ between differentially charged PS-treated and control mice. Interestingly, the expression of *zonula occludens* (*ZO-1*) mRNA in the noncharged PS-treated mice was significantly higher than that in the control mice. A significant downregulation of *ZO-1* expression was observed in the colon of the mice in the PS-NH₂ and PS-COOH groups compared with noncharged PS group.

Fecal samples were harvested at nine weeks to assess the composition of the gut microbiota. Compared with the CK treatment, differentially charged PS with changed the relative abundances of bacterial taxa at the phylum level (Fig. 2A). PS- and PS-COOH-treated mice showed significant increases in the abundance of *Proteobacteria*. At the genus level, PS-NH₂ or PS-COOH treatment increased the abundance of *Helicobacter* (Fig. 2B). A PCoA of species revealed that although all samples of the vehicle-treated group clustered similarly, exposure to differentially charged PS for nine weeks drastically altered the gut microbial profile (Fig. 2C). The common and unique species of each group were analyzed and are presented in a Venn diagram (Fig. 2D).

To investigate the relationship between the fecal metabolome and intestinal impairment induced by differentially charged PS, untargeted metabolomic profiling through metabolomic analysis was performed

(Fig. 3). First, low-abundance signals were filtered out. All of the identified metabolites were classified and counted according to their chemical taxonomy, and the proportions of various metabolites are shown in Fig. 3A. In total, 237 metabolites were found to be significantly altered in the differentially charged PS-treated groups compared with the control (Table S2). A PCA plot revealed the distribution of significantly altered metabolites after exposure to differentially charged PS treatments (Fig. 3B). The numbers of significantly altered metabolites identified from five comparisons were further investigated. The PS vs. CK, PS-NH₂ vs. CK, and PS-COOH vs. CK comparisons indicated that differentially charged PS induced significant fecal metabolic alterations, and the PS-NH₂ vs. PS and PS-COOH vs. PS comparisons indicated that negative or positive charges on PS-NPs further affected these metabolic changes (Fig. 3C). The volcano plot of the significantly altered metabolites of PS-COOH vs. the control, PS-COOH vs. PS, PS-NH₂ vs. CK, PS-NH₂ vs. PS, and PS vs. CK are shown in Fig. S1. The predictive accuracy of 237 metabolites was used to distinguish between the differentially charged PS and the normal individuals. Based on the relative abundances detected by untargeted metabolomic profiling, the vehicle group and intestinal inflammatory individuals with the PS, PS-NH₂, and PS-COOH exposure could be accurately distinguished (all AUCs > 0.5), with AUCs reaching of 0.61, 0.58, and 0.59, respectively (Fig. 3D).

Spearman's correlation coefficient analysis was carried out using data on fecal metabolites and gut microbiome species in differentially charged PS-treated mice with intestinal impairment (Fig. S2, Table S3).

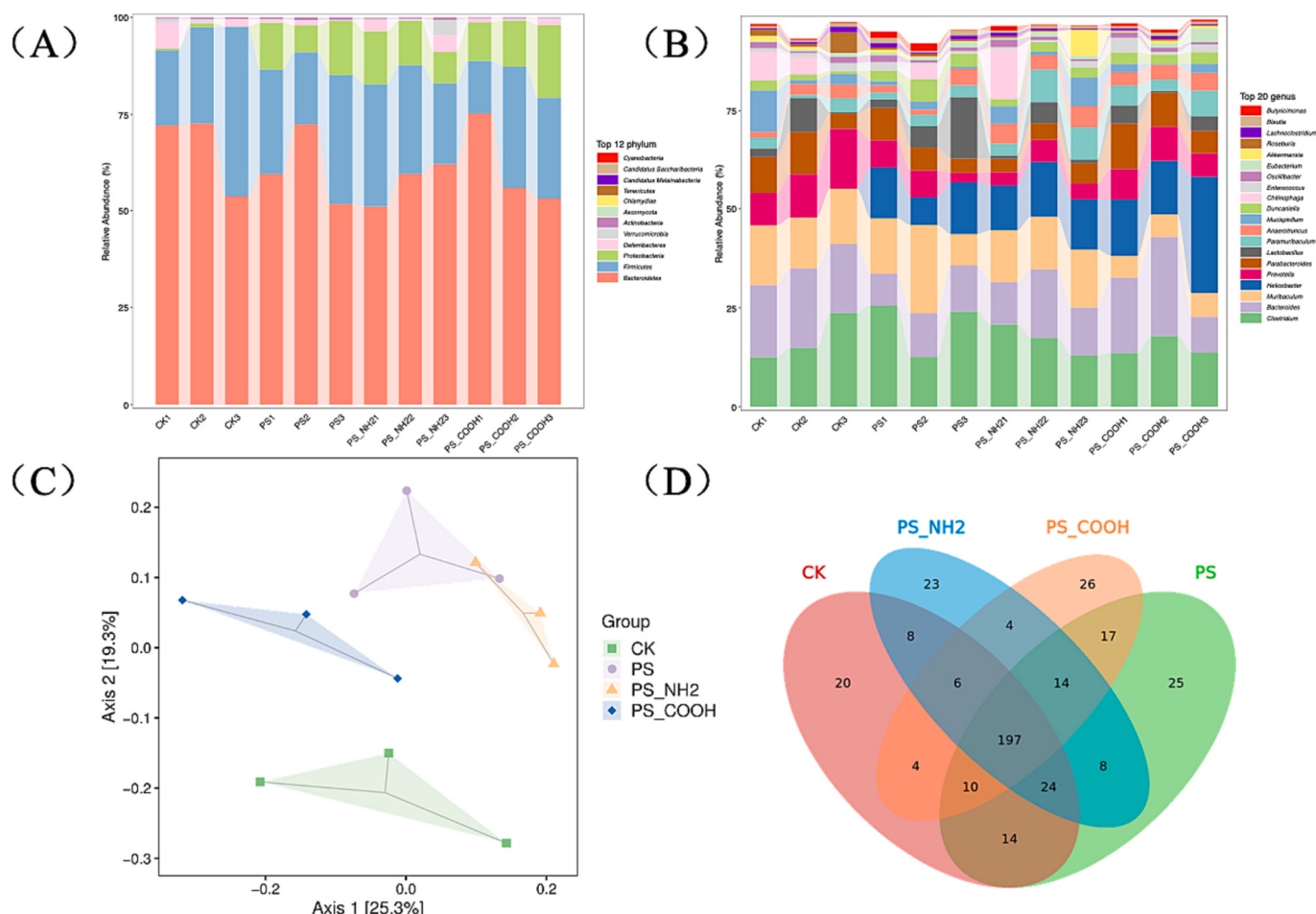


Fig. 2. Alterations in the gut microbiome of male mice exposed to PS, PS-NH₂, and PS-COOH determined by metagenome analysis (n = 3 mice per group). A. Comparison of the relative abundances of bacterial taxa at the phylum level between the differentially charged PS-treated and control mice. B. Comparison of the relative abundances of bacterial taxa at the genus level between the differentially charged PS-treated and control mice. C. A principal coordinate analysis (PCoA) of species based on unweighted UniFrac distances between differentially charged PS-treated and control mice. D. A Venn diagram showing the number of species in the CK, PS, PS-NH₂, and PS-COOH groups.

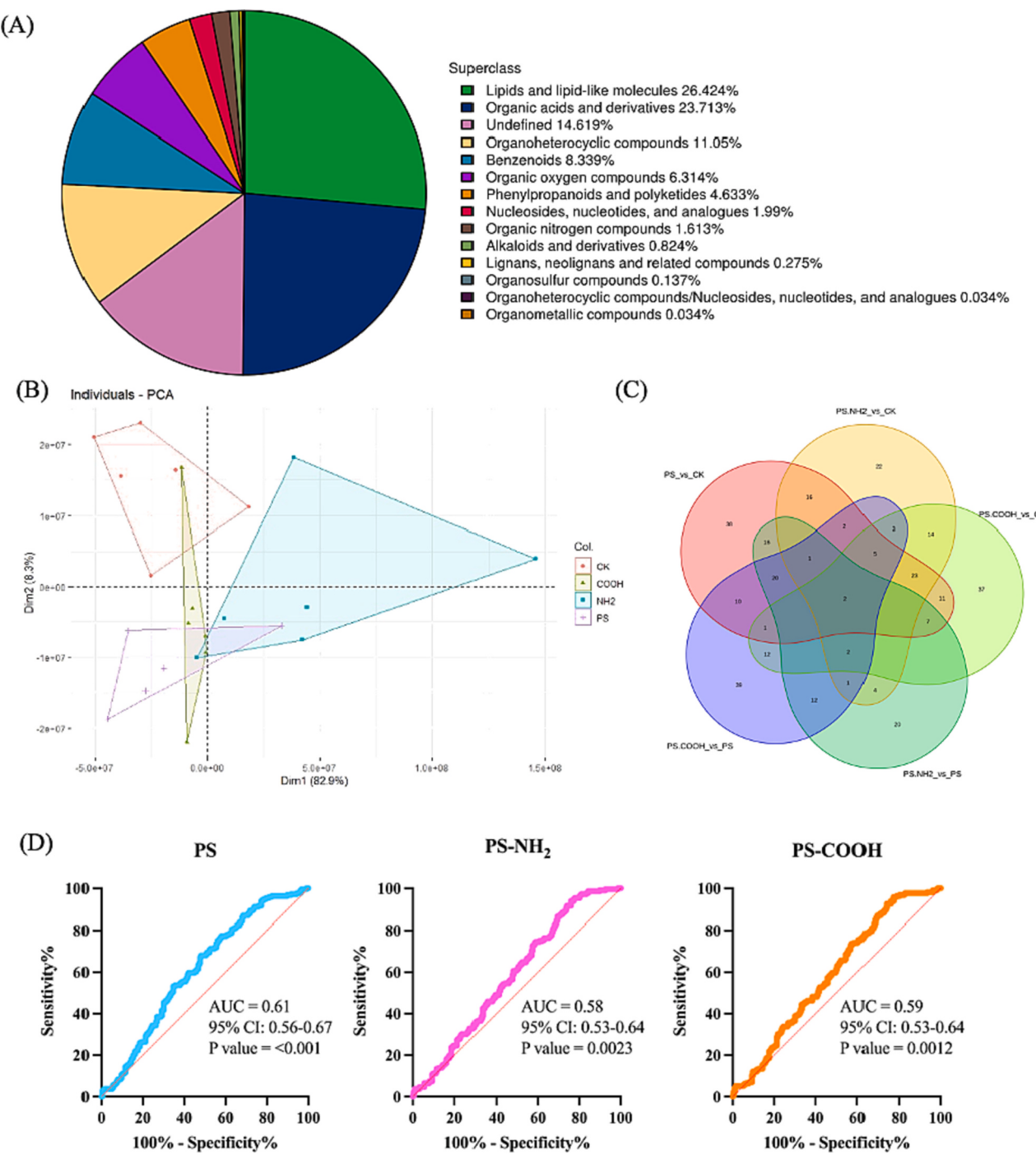


Fig. 3. Overview of changes in the fecal metabolome of mice following exposure to PS, PS-NH₂, and PS-COOH compared with the control group. A. The number of identified metabolites in each chemical taxonomy. B. A PCA plot showing the significant alterations of fecal metabolites induced by exposure to PS, PS-NH₂, and PS-COOH. C. A Venn diagram showing the overlaps between significantly altered metabolites in the five comparison pairs (PS vs. CK, PS-NH₂ vs. CK, PS-COOH vs. CK, PS-NH₂ vs. PS, and PS-COOH vs. PS). D. ROC curve of differences in the gut microbiome-associated fecal metabolites among the PS, PS-NH₂, PS-COOH and CK groups based on significantly differentially accumulated metabolites identified by untargeted metabolomic analysis.

Among the correlated metabolite-species pairs, 216 metabolites exhibited a significant association with 33 species of the gut microbiome. A correlation network between significantly altered metabolites and species based on Spearman's correlation coefficient ($|\rho| > 0.8$, P value < 0.01) was constructed using Mothur software and visualized using Cytoscape software (Fig. S2B).

To further confirm the relationship between the fecal metabolites and the gut microbiome, we used secondary bile acids that are known to participate in the regulation of the gut microbiome and intestinal

inflammation (Cai et al., 2022; Sinha et al., 2020), such as isodeoxycholic acid, and *Bilophila-wadsworthia* (Fig. S1C, D). Spearman's correlation coefficient between isodeoxycholic acid and *Bilophila wadsworthia* was found to be 0.62 (P value = 0.032). We further evaluated metabolite correlations with the nongastric *Helicobacter* species *Helicobacter apodemus*, and *Helicobacter typhlonius*, whose gastric introduction has been reported to induce gut inflammation and disrupted gut homeostasis (Bostick et al., 2019). Taurocholate was found to be significantly negatively correlated with both *Helicobacter apodemus* and

Helicobacter typhlonius (Table S3).

From the 216 gut microbiome-associated fecal metabolites described above, key biomarkers for predicting intestinal inflammation after exposure to differentially charged PS were identified using the LASSO algorithm. The LASSO analysis model filtered 10 potential metabolites (Table S4). The PCA plot in Fig. 4B shows a clear discrimination between the PS, PS-NH₂, PS-COOH, and CK groups based on significant alterations in the levels of 10 gut microbiome-associated fecal metabolites identified by untargeted metabolomic analysis. Compared with the CK treatment, exposure to noncharged PS-NPs increased the relative levels of 1-myristoyl-sn-glycero-3-phosphocholine (14:0 Lyso PC), 1-palmitoyl-2-hydroxy-sn-glycero-3-phospho-(1'-rac-glycerol) (16:0 Lyso PG), and flumethasone pivalate and decreased the levels of ethylenediaminetetraacetic acid and D-proline; exposure to PS-NH₂ increased the levels of 1-myristoyl-sn-glycero-3-phosphocholine and deoxycholic acid and decreased the levels of D-proline; and exposure to PS-COOH significantly increased the levels of 7 metabolites, namely 1-myristoyl-sn-glycero-3-phosphocholine, indoleacetic acid, 1-palmitoyl-2-hydroxy-sn-glycero-3-phospho-(1'-rac-glycerol), alpha-tochopheryl acetate, flumethasone pivalate, glabridin, and pristimerin (Table S4, Fig. 4C). Specifically, compared with the results obtained after exposure to noncharged PS-NPs, exposure to positively charged PS (PS-NH₂) increased the levels of deoxycholic acid, whereas exposure to negatively charged PS (PS-COOH) increased the levels of indoleacetic acid and pristimerin (Fig. 4C).

We subsequently evaluated the predictive accuracy of the metabolite panel for distinguishing between mice with intestinal impairment after exposure to differentially charged PS and CK mice. A model based on the 10 significantly altered metabolites identified in untargeted metabolomic analysis was evaluated. The alterations in the concentrations of three metabolites (1-myristoyl-sn-glycero-3-phosphocholine, deoxycholic acid, and indoleacetic acid) identified by targeted metabolomics were consistent with those identified by untargeted metabolomics (Fig. S2). The results showed that the particular metabolites 1-myristoyl-sn-glycero-3-phosphocholine, deoxycholic acid, and indoleacetic acid achieved better AUCs of 1.0, 0.94, and 0.86, respectively, after exposure to PS, PS-NH₂, and PS-COOH, which revealed significant accuracy (Fig. 4D).

4. Discussion

In this study, we performed untargeted metabolomic analysis to establish a biomarker model for detecting intestinal impairment after exposure to differentially charged PS-NPs. Our model based on specific fecal metabolites showed high accuracy for detecting intestinal changes in response to PS-NPs with negative or positive charges. The findings suggest that this panel of gut microbiome-associated fecal metabolites could be a promising tool for detecting intestinal impairment in organisms following exposure to differentially charged NPs.

Recent studies have proposed that environmental factors may induce an inflammatory response, immune dysbiosis, neurotoxicity, and cancer via different mechanisms (Duntas, 2008; Kawaguchi et al., 2016; Santos et al., 2022; Voth-Gaeddert et al., 2019). Although an accurate detection of potential intestinal impairments induced by environmental factors is challenging, a certain factor is generally considered toxic if it elicits inflammatory responses, such as inhibiting the expression of anti-inflammatory interleukins (ILs) (Ryzhakov et al., 2018; Shouval et al., 2016). In the present study, the downregulation of *IL-1b*, *IL-6*, and *IL-10* mRNA expression in mice after exposure to differentially charged PS-NPs resulted in intestinal impairment. Polyvinyl chloride MPs and NPs as toxicants have been shown to decrease the concentration of IL-8 in the basolateral compartment of the mouse intestine, resulting in intestinal inflammation (Busch et al., 2021). The upregulation of *TNFα* was observed after differentially charged PS-NP treatment. This result is consistent with the previous findings that exposure to 20 and 100 µg/L PS significantly increased *TNFα* expression in the zebrafish intestine

(Teng et al., 2022a; Yu et al., 2022).

The intestinal mucus layer and Toll-like receptors, which serve as a physical barrier, constitute the innate defense of the immune system against viruses, pathogenic bacteria, and harmful exogenous factors (Johansson et al., 2008; Zhou et al., 2007). Muc2, the most abundantly secreted mucin in the intestine, is a heavily O-glycosylated glycoprotein that is characteristically large and conducive to the specific properties of the intestinal mucus layer. Previous studies have shown that Muc2 and TLR3 signaling disrupts mucosal homeostasis (Velcich et al., 2002; Zhou et al., 2007). Tff-3 is predominantly expressed in the goblet cells of the colon and plays a critical role in mucosal regeneration and repair and in maintaining epithelial homeostasis in the colon (Mashimo et al., 1996). Studies have revealed that Tff-3-knockout mice exhibit increased epithelial apoptosis and proliferation, leading to a normal crypt appearance (Aihara et al., 2017; Mashimo et al., 1996). IFN γ inhibits intestinal restitution by preventing gap junction communication between enterocytes (Leaphart et al., 2007). The dysregulation of *Muc2*, *TLR3*, *Tff-3*, and *IFN γ* expression results in epithelial cell damage and immune responses.

The intestinal epithelial cells are a crucial component of the barrier against external factors. Epithelial cell damage facilitates external factors to cross the intestine and interfere with the homeostasis of the gut microbiome (Allen and Sears, 2019). The gut microbiome, which is the largest microbial community and represents a vast metabolic capacity of the intestine, is known to be affected by extrinsic factors (Lindell et al., 2022). The complex composition of the gut microbial community plays an important role in the immune responses and biological metabolism influencing host health. Proteobacteria, which are gram-negative bacteria, contribute to alterations in the host metabolism (Shin et al., 2015). An unstable intestinal microbiota, particularly due to an increase in the relative abundance of *Proteobacteria*, predisposes genetically susceptible mice to chronic colitis (Carvalho et al., 2012). Due to intolerance of the gut microbiota, IL-10-deficient mice develop spontaneous colitis. These findings suggest that the imbalance of innate immune responses promotes increases in the abundance of *Proteobacteria*, which in turn drives intestinal inflammation (Maharshak et al., 2013). *Helicobacter*, a member of the gut microbiota, is tolerated by the host and is a bacterial pathogen responsible for gastrointestinal morbidity (Cao, 2017; Xu et al., 2018). In this study, the downregulation of *IL-10* expression dysregulated the innate and adaptive immune systems, damaged the epithelial cell structure and induced inflammatory cell infiltration, increased the relative abundance of *Proteobacteria* in PS and PS-COOH-treated mice, and increased the relative abundance of *Helicobacter* in PS-NH₂- and PS-COOH-treated mice.

Previous studies have investigated serum- or feces-based metabolite panels but only compared the serum or fecal metabolome between normal organisms and organisms with intestinal impairment after chemical exposure (Kim et al., 2020; Yan et al., 2021). The gut microbiome-associated fecal metabolite panel should consist of important metabolites that could be considered outcomes of intestinal impairment-related changes in the gut microbiome. The microbiota composition accounts for approximately 68 % of the gut metabolome, including some gut microbiota-related metabolites detected in the feces and serum (Han et al., 2021; Zierer et al., 2018). In addition, positively charged NPs (PS-NH₂) can translocate across cell membranes with more favorable electrostatic interactions and destroy the cell membrane of gram-positive bacteria, while PS and PS-COOH show much less efficacy in translocation (Dai et al., 2022; Teng et al., 2022c). Therefore, it is important to understand how various environmental factors affect the gut microbiota and its metabolism. Several gut microbiota-associated metabolic pathways, such as bile acid metabolism, tryptophan metabolism, and lipid metabolism, have been investigated in organisms with intestinal impairments following exposure to environmental contaminants (Bauermeister et al., 2021; Funabashi et al., 2020; Han et al., 2021; Visconti et al., 2019). The key metabolites that are produced by microbes or derived from environmental or host molecule

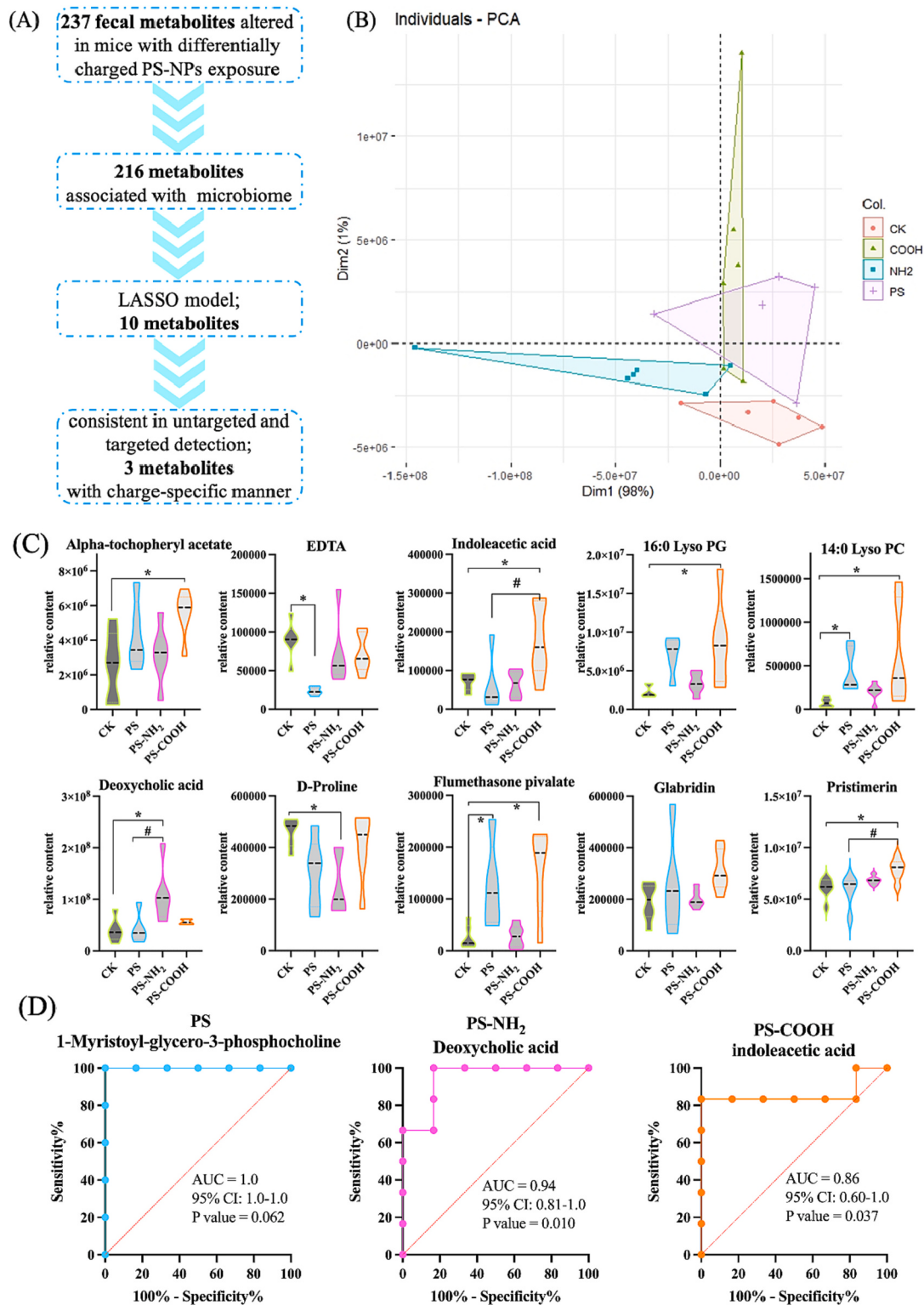


Fig. 4. A panel of gut microbiome-associated fecal metabolites could predict gut impairment induced by differentially charged PS. The LASSO algorithm was further used to select key metabolites. Ten metabolites were found to exhibit significant variances by untargeted metabolomic analysis and were selected for further model construction. A. Diagram representing the process used for fecal metabolite selection. B. A PCA plot showing clear discrimination between the PS, PS-NH₂, PS-COOH, and CK groups based on significant alterations in fecal metabolites. C. Relative contents of several metabolites in the CK, PS, PS-NH₂, and PS-COOH groups. The data are expressed as the mean \pm SD. * $P < 0.05$ vs. the CK group, and # $P < 0.05$ vs. the PS group. D. ROC curve of specific metabolites after exposure to PS, PS-NH₂, and PS-COOH based on untargeted metabolomic analysis of feces for the discrimination between the PS, PS-NH₂, PS-COOH, and the control groups.

transformation mediate physiological changes in the host. The conjugated bile acids are secreted by the liver tissue and deconjugated by the gut microbiomes with bile salt hydrolase activity. Certain bacterial species, including *Clostridiaceae* and *Eggerthella* spp., encode the bile acid-inducible gene cluster and convert free unconjugated primary bile acid into deoxycholic acid. The abovementioned bile acids can be reabsorbed and aid fat absorption in the intestine and then modulate the inflammatory response of the liver and other tissues (Heinken et al., 2019; Jiao et al., 2018). In this study, increased levels of deoxycholic acid activated the immune response in the mouse gut after PS-NH₂ exposure. Tryptophan, an essential aromatic acid, is a biosynthetic precursor of microbial and host metabolites (Agus et al., 2018). In the gut, the intestinal microbiota transforms tryptophan into molecules such as indole and its derivatives, which are ligands for the aryl hydrocarbon receptor, and thus regulate immune responses and intestinal homeostasis (Schiering et al., 2017). Indole and its derivatives can regulate bacterial physiology and inhibit quorum sensing. Indoleacetic acid, a metabolite of tryptophan metabolism, influences host immunity and intestinal permeability. We found that the dysregulation of indoleacetic acid in PS-COOH-treated mice affected gut permeability, disturbed the homeostasis of microbial immunity, and resulted in intestinal impairment. Physiologically, the absence of immune cells impairs host lipid metabolism by decreasing lipid transporter expression (Mao et al., 2018). In addition, studies have revealed that *Bilophila-wadsworthia* promotes intestinal barrier dysfunction and high inflammation, resulting in high glucose dysmetabolism (Natividad et al., 2018). A previous study reported on overgrowth of *Bilophila-wadsworthia* and the inducing of proinflammatory mucosal immune responses in IL-10-deficient mice that were fed with a rich saturated-milk-fat diet (David et al., 2013; Devkota et al., 2012). Consistently, in the PS-exposed group, the downregulation of *IL-10* expression induced an overgrowth of *Bilophila-wadsworthia* and led to intestinal inflammation. The concentration of isodeoxycholic acid in the feces was increased in mice after PS exposure relative to vehicle-control-treated mice. The correlation between bile acids and gut microbiome species revealed that the abundance of *Bilophila-wadsworthia* was significantly positively correlated with the level of isodeoxycholic acid and that the level of taurocholate was significantly negatively correlated with the abundances of *Helicobacter apodemus* and *Helicobacter typhlonius*. These species were also overrepresented in mice with intestinal impairment following exposure to PS and PS-COOH, which is consistent with the results from previous studies on populations with intestinal impairment (Bostick et al., 2019; Varon et al., 2021) (Lee et al., 2020; Lindell et al., 2022).

Furthermore, focusing on the gut microbiome-associated fecal metabolites, we identified a panel of fecal metabolites sensitive to intestinal inflammation caused by differentially charged PS, thus providing a promising tool for detecting intestinal impairment in an NPs charge-specific manner. After exposure to noncharged PS, 1-myristoyl-sn-glycero-3-phosphocholine (14:0 Lyso PC), a crucial metabolite in lipid metabolism, could achieve a high AUC of 1.0 in mice with intestinal impairment. Our model achieved a high AUC of 0.94 because this specific metabolite plays a significant role in bile acid metabolism and is associated with the relative abundance of deoxycholic acid in mice after exposure to positively charged PS (PS-NH₂). Negatively charged PS (PS-COOH) achieved a good AUC based on the relative abundance of indoleacetic acid, which participates in tryptophan metabolism.

5. Conclusion

In this study, using combined analyses of the gut metagenome and the fecal metabolome of mice showing intestinal impairment after exposure to differentially charged PS and of normal mice subjected to vehicle-control treatment, we uncovered the link between the gut microbiome composition and fecal metabolic profiles. The study established a metabolite-based model with high accuracy for predicting the intestinal impairment in response to exposure to charge-specific NPs.

Our results provide evidence that the effects of NPs on the host metabolism differ depending on their surface charges. Differentially charged PS can have direct health outcomes, in addition to impacting ecological sustainability.

CRediT authorship contribution statement

M. T., L. Z., J. S., X. Z., and F. W. contributed to the literature search. M. T. and F. W. designed the study. M. T., L. Z., J. S., Y. L., and W. Z. performed the experiments. M. T., L. Zhou, and H. Y. analyzed the data. M. T. and X. Z. made the Figs. M. T., F. W., H. Y., and X. Z. wrote and corrected the manuscript. All authors reviewed and approved the final manuscript.

Declaration of competing interest

The authors declare that they have no known competing financial interests or personal relationships that could have appeared to influence the work reported in this paper.

Data availability

The data that support the findings of this study are reviewed in <https://dataview.ncbi.nlm.nih.gov/object/PRJNA863263?reviewer=45pvuu834t2m2b834jm7ns1eud> [ncbi.nlm.nih.gov].

Acknowledgements

This work was supported by the National Natural Science Foundation of China [grant number 42207335], the National Science Fund for Distinguished Young Scholars [grant number 41925031], the National Key Research and Development Program of China [grant number 2021YFC3201000] and Young Elite Scientists Sponsorship Program by CAST [grant number 2022QNRC001]. We thank Personal Biotechnology Co., Ltd. (Shanghai, China) for detecting metagenomics and metabolomics profile.

Appendix A. Supplementary data

Supplementary data to this article can be found online at <https://doi.org/10.1016/j.scitotenv.2023.167287>.

References

- Agirman, G., Yu, K.B., Hsiao, E.Y., 2021. Signaling inflammation across the gut-brain axis. *Science* 374, 1087–1092.
- Agus, A., Planchais, J., Sokol, H., 2018. Gut microbiota regulation of tryptophan metabolism in health and disease. *Cell Host Microbe* 23, 716–724.
- Aihara, E., Engevik, K.A., Montrose, M.H., 2017. Trefoil factor peptides and gastrointestinal function. *Annu. Rev. Physiol.* 79, 357–380.
- Allen, J., Sears, C.L., 2019. Impact of the gut microbiome on the genome and epigenome of colon epithelial cells: contributions to colorectal cancer development. *Genome Med.* 11, 11.
- Al-Sid-Cheikh, M., Rowland, S.J., Stevenson, K., Rouleau, C., Henry, T.B., Thompson, R.C., 2018. Uptake, whole-body distribution, and depuration of nanoplastics by the scallop *Pecten maximus* at environmentally realistic concentrations. *Environ. Sci. Technol.* 52, 14480–14486.
- Bauermeister, A., Mannochio-Russo, H., Costa-Lotufo, L.V., Jarmusch, A.K., Dorrestein, P.C., 2021. Mass spectrometry-based metabolomics in microbiome investigations. *Nat. Rev. Microbiol.* 20, 143–160.
- Bostick, J.W., Wang, Y., Shen, Z., Ge, Y., Brown, J., Chen, Z.-M.E., et al., 2019. Dichotomous regulation of group 3 innate lymphoid cells by nongastric *Helicobacter* species. *Proc. Natl. Acad. Sci. U. S. A.* 116, 24760–24769.
- Busch, M., Bredeck, G., Kämpfer, A.A.M., Schins, R.P.F., 2021. Investigations of acute effects of polystyrene and polyvinyl chloride micro- and nanoplastics in an advanced in vitro triple culture model of the healthy and inflamed intestine. *Environ. Res.* 193, 110536.
- C., D.T., Bergami, E., Salvati, A., Falieri, C., Cirino, P., Dawson, K.A., et al., 2014. Accumulation and embryotoxicity of polystyrene nanoparticles at early stage of development of sea urchin embryos *Paracentrotus lividus*. *Environ. Sci. Technol.* 48, 12302–12311.

- Cai, J., Sun, L., Gonzalez, F.J., 2022. Gut microbiota-derived bile acids in intestinal immunity, inflammation, and tumorigenesis. *Cell Host Microbe* 30, 289–300.
- Cani, P.D., 2019. Microbiota and metabolites in metabolic diseases. *Nat. Rev. Endocrinol.* 15, 69–70.
- Cao, X., 2017. Intestinal inflammation induced by oral bacteria. *Science* 258, 308–309.
- Carvalho, F.A., Koren, O., Goodrich, J.K., Johansson, M.E.V., Nalbantoglu, I., Aitken, J. D., et al., 2012. Transient inability to manage proteobacteria promotes chronic gut inflammation in TLR5-deficient mice. *Cell Host Microbe* 12, 139–152.
- Casado, M.P., Macken, A., Byrne, H.J., 2012. Ecotoxicological assessment of silica and polystyrene nanoparticles assessed by a multirisk test battery. *Environ. Int.* 97–105.
- Chen, J., Chen, X., Xuan, Y., Shen, H., Tang, Y., Zhang, T., et al., 2023a. Surface functionalization-dependent inflammatory potential of polystyrene nanoplastics through the activation of MAPK/ NF- κ B signaling pathways in macrophage Raw 264.7. *Ecotoxicol. Environ. Saf.* 117884.
- Chen, J., Chen, X., Xuan, Y., Shen, H., Tang, Y., Zhang, T., et al., 2023b. Surface functionalization-dependent inflammatory potential of polystyrene nanoplastics through the activation of MAPK/ NF- κ B signaling pathways in macrophage raw 264.7. *Ecotoxicol. Environ. Saf.* 114520.
- Coryell, M., McAlpine, M., Pinkham, N.V., McDermott, T.R., Walk, S.T., 2018. The gut microbiome is required for full protection against acute arsenic toxicity in mouse models. *Nat. Commun.* 9, 5424.
- Dai, S., Ye, R., Huang, J., Wang, B., Xie, Z., Ou, X., et al., 2022. Distinct lipid membrane interaction and uptake of differentially charged nanoplastics in bacteria. *J. Nanobiotechnology*, 20, 191.
- David, L.A., Maurice, C.F., Carmody, R.N., Gootenberg, D.B., Button, J.E., Wolfe, B.E., et al., 2013. Diet rapidly and reproducibly alters the human gut microbiome. *Nature* 505, 559–563.
- Desai, M.S., Seekatz, A.M., Koropatkin, N.M., Kamada, N., Hickey, C.A., Wolter, M., et al., 2016. A dietary fiber-deprived gut microbiota degrades the colonic mucus barrier and enhances pathogen susceptibility. *Cell* 167, 1339–1353.E21.
- Devkota, S., Wang, Y., Musch, M.W., Leone, V., Fehlner-Peach, H., Nadimpalli, A., et al., 2012. Dietary fat-induced taurocholic acid promotes pathobiont expansion and colitis in IL10 $^{-/-}$ mice. *Nature* 487, 104–108.
- Duntas, L.H., 2008. Environmental factors and autoimmune thyroiditis. *Nat. Rev. Endocrinol.* 4, 454–460.
- Fan, Y., Pedersen, O., 2021. Gut microbiota in human metabolic health and disease. *Nat. Rev. Microbiol.* 19, 55–71.
- Funabashi, M., Grove, T.L., Wang, M., Varma, Y., McFadden, M.E., Brown, L.C., et al., 2020. A metabolic pathway for bile acid dehydroxylation by the gut microbiome. *Nature* 582, 566–570.
- Gao, Y., Dong, Y., Yang, S., Mo, A., Zeng, X., Chen, Q., et al., 2022. Size-dependent photothermal antibacterial activity of Ti3C2Tx MXene nanosheets against methicillin-resistant *Staphylococcus aureus*. *J. Colloid Interface Sci.* 617, 533–541.
- Garrett, W.S., 2020. Immune recognition of microbial metabolites. *Nat. Rev. Immunol.* 20, 91–92.
- Han, S., Van Treuren, W., Fischer, C.R., Merrill, B.D., DeFelice, B.C., Sanchez, J.M., et al., 2021. A metabolomics pipeline for the mechanistic interrogation of the gut microbiome. *Nature* 595, 415–420.
- Heinken, A., Ravcheev, D.A., Baldini, F., Heirendt, L., Fleming, R.M.T., Thiele, I., 2019. Systematic assessment of secondary bile acid metabolism in gut microbes reveals distinct metabolic capabilities in inflammatory bowel disease. *Microbiome* 7, 75.
- Huang, F., Zheng, X., Ma, X., Jiang, R., Zhou, W., Zhou, S., et al., 2019. Theabrownin from Pu-erh tea attenuates hypercholesterolemia via modulation of gut microbiota and bile acid metabolism. *Nat. Commun.* 10, 4971.
- Jacob, H., Besson, M., Swarzenski, P.W., Lecchini, D., Metian, M., 2020. Effects of virgin micro- and nanoplastics on fish: trends, meta-analysis, and perspectives. *Environ. Sci. Technol.* 54, 4733–4745.
- Jenner, L.C., Rotchell, J.M., Bennett, R.T., Cowen, M., Tentzeris, V., Sadofsky, L.R., 2022. Detection of nanoplastics in human lung tissue using μ FTIR spectroscopy. *Sci. Total Environ.* 831, 154907.
- Jiao, N., Baker, S.S., Chapa-Rodriguez, A., Liu, W., Nugent, C.A., Tsompana, M., et al., 2018. Suppressed hepatic bile acid signalling despite elevated production of primary and secondary bile acids in NAFLD. *Gut* 67, 1881.
- Johansson, M.E.V., Phillipson, M., Petersson, J., Velcich, A., Holm, L., Hansson, G.C., 2008. The inner of the two Muc2 mucin-dependent mucus layers in colon is devoid of bacteria. *Proc. Natl. Acad. Sci. U. S. A.* 105, 15064–15069.
- Kawaguchi, T., Koh, Y., Ando, M., Ito, N., Takeo, S., Adachi, H., et al., 2016. Prospective analysis of oncogenic driver mutations and environmental factors: Japan molecular epidemiology for lung cancer study. *J. Clin. Oncol.* 34, 2247–2257.
- Kim, H.M., Long, N.P., Min, J.E., Anh, N.H., Kim, S.J., Yoon, S.J., et al., 2020. Comprehensive phenotyping and multi-omic profiling in the toxicity assessment of nanopolystyrene with different surface properties. *J. Hazard. Mater.* 399, 123005.
- Leaphart, C.L., Qureshi, F., Cetin, S., Li, J., Dubowski, T., Baty, C., et al., 2007. Interferon-gamma inhibits intestinal restitution by preventing gap junction communication between enterocytes. *Gastroenterology* 132, 2395–2411.
- Lee, G., You, H.J., Bajaj, J.S., Joo, S.K., Yu, J., Park, S., et al., 2020. Distinct signatures of gut microbiome and metabolites associated with significant fibrosis in non-obese NAFLD. *Nat. Commun.* 11, 4982.
- Lenz, R., Enders, K., Nielsen, T.G., 2016. Microplastic exposure studies should be environmentally realistic [biological sciences]. *Proc. Natl. Acad. Sci. U. S. A.* 113, E4121–E4122.
- Leslie, H.A., van Velzen, M.J.M., Brandsma, S.H., Vethaak, A.D., Garcia-Vallejo, J.J., Lamoree, M.H., 2022. Discovery and quantification of plastic particle pollution in human blood. *Environ. Int.* 163, 107199.
- Li, X., Brejnrod, A.D., Ernst, M., Rykær, M., Herschend, J., Olsen, N.M.C., et al., 2019. Heavy metal exposure causes changes in the metabolic health-associated gut microbiome and metabolites. *Environ. Int.* 126, 454–467.
- Li, Y., Liu, Y., Liu, S., Zhang, L., Shao, H., Wang, X., et al., 2022. Photoaging of baby bottle-derived polyethersulfone and polyphenylsulfone nanoplastics and the resulting bisphenol S release. *Environ. Sci. Technol.* 56, 3033–3044.
- Lin, X., Zhao, J., Zhang, W., He, L., Wang, L., Li, H., et al., 2021. Towards screening the neurotoxicity of chemicals through feces after exposure to methylmercury or inorganic mercury in rats: a combined study using gut microbiome, metabolomics and metallomics. *J. Hazard. Mater.* 409, 124923.
- Lindell, A.E., Zimmermann-Kogadeeva, M., Patil, K.R., 2022. Multimodal interactions of drugs, natural compounds and pollutants with the gut microbiota. *Nat. Rev. Microbiol.* 20, 431–443.
- Luo, H., Liu, C., He, D., Xu, J., Sun, J., Li, J., et al., 2022. Environmental behaviors of nanoplastics in aquatic systems: a systematic review on degradation, adsorption, toxicity and biofilm under aging conditions. *J. Hazard. Mater.* 423, 126915.
- Lynch, J.B., Hsiao, E.Y., 2019. Microbiomes as sources of emergent host phenotypes. *Science* 365, 1405–1409.
- Maharshak, N., Packey, C.D., Ellermann, M., Manick, S., Siddle, J.P., Huh, E.Y., et al., 2013. Altered enteric microbiota ecology in interleukin 10-deficient mice during development and progression of intestinal inflammation. *Gut Microbes* 4, 316–324.
- Maloy, K.J., Powrie, F., 2011. Intestinal homeostasis and its breakdown in inflammatory bowel disease. *Nature* 474, 298–306.
- Mao, K., Baptista, A.P., Tamoutounour, S., Zhuang, L., Bouladoux, N., Martins, A.J., et al., 2018. Innate and adaptive lymphocytes sequentially shape the gut microbiota and lipid metabolism. *Nature* 554, 255–259.
- Mashimo, H., Wu, D.-C., Podolsky, D.K., Fishman, M.C., 1996. Impaired defense of intestinal mucosa in mice lacking intestinal trefoil factor. *Science* 274 (5285), 262–265.
- Natividad, J.M., Lamas, B., Pham, H.P., Michel, M.-L., Rainteau, D., Bridonneau, C., et al., 2018. *Bilophila wadsworthia* aggravates high fat diet induced metabolic dysfunctions in mice. *Nat. Commun.* 9, 2802.
- Qiao, J., Chen, R., Wang, M., Bai, R., Cui, X., Liu, Y., et al., 2021. Perturbation of gut microbiota plays an important role in micro/nanoplastics-induced gut barrier dysfunction. *Nanoscale* 8806–8816.
- Rakoff-Nahoum, S., Foster, K.R., Comstock, L.E., 2016. The evolution of cooperation within the gut microbiota. *Nature* 533, 255–259.
- Raskov, H., Burchart, J., Pommergaard, H.-C., Rosenberg, J., 2016. Irritable bowel syndrome, the microbiota and the gut-brain axis. *Gut Microbes* 7, 365–383.
- Rooks, M.G., Garrett, W.S., 2016. Gut microbiota, metabolites and host immunity. *Nat. Rev. Immunol.* 16, 341–352.
- Ryzhakov, G., West, N.R., Franchini, F., Clare, S., Illott, N.E., Sansom, S.N., et al., 2018. Alpha kinase 1 controls intestinal inflammation by suppressing the IL-12/Th1 axis. *Nat. Commun.* 9, 3797.
- Santos, A.L., Rodrigues, C.C., Oliveira, M., Rocha, T.L., 2022. Microbiome: a forgotten target of environmental micro(nano)plastics? *Sci. Total Environ.* 822, 153628.
- Schiering, C., Wincent, E., Metidji, A., Iseppon, A., Li, Y., Potocnik, A.J., et al., 2017. Feedback control of AHR signalling regulates intestinal immunity. *Nature* 542, 242–245.
- Shin, N.-R., Whon, T.W., Bae, J.-W., 2015. Proteobacteria: microbial signature of dysbiosis in gut microbiota. *Trends Biotechnol.* 33, 496–503.
- Shouval, D.S., Biswas, A., Kang, Y.H., Griffith, A.E., Konnikova, L., Mascanfroni, I.D., et al., 2016. Interleukin 1 β mediates intestinal inflammation in mice and patients with interleukin 10 receptor deficiency. *Gastroenterology* 151, 1100–1104.
- Simon, N., Raubenheimer, K., Urho, N., Unger, S., Azoulay, D., Farrelly, T., et al., 2021. A binding global agreement to address the life cycle of plastics. *Science* 373, 43–47.
- Sinha, S.R., Haileslassie, Y., Nguyen, L.P., Tropini, C., Wang, M., Becker, L.S., et al., 2020. Dysbiosis-induced secondary bile acid deficiency promotes intestinal inflammation. *Cell Host Microbe* 27, 659–670 (e5).
- Sonnenburg, J.L., Bäckhed, F., 2016. Diet-microbiota interactions as moderators of human metabolism. *Nature* 535, 56–64.
- Teng, M., Zhao, X., Wang, C., Wang, C., White, J.C., Zhao, W., et al., 2022a. Polystyrene nanoplastics toxicity to zebrafish: dysregulation of the brain-intestine-microbiota axis. *ACS Nano* 16, 8190–8204.
- Teng, M., Zhao, X., Wu, F., Wang, C., Wang, C., White, J.C., et al., 2022b. Charge-specific adverse effects of polystyrene nanoplastics on zebrafish (*Danio rerio*) development and behavior. *Environ. Int.* 163, 107154.
- Teng, M., Zhao, X., Wu, F., Wang, C., Wang, C., White, J.C., et al., 2022c. Charge-specific adverse effects of polystyrene nanoplastics on zebrafish (*Danio rerio*) development and behavior. *Environ. Int.* 163, 107154.
- Varon, C., Azzi-Martin, L., Khalid, S., Seenevassen, L., Ménard, A., Spuul, P., 2021. Helicobacters and cancer, not only gastric cancer? *Semin. Cancer Biol.* 86 (2), 1138–1154.
- Velcich, A., Yang, W., Heyer, J., Fragale, A., Nicholas, C., Viani, S., et al., 2002. Colorectal cancer in mice genetically deficient in the mucin Muc2. *Science* 295, 1726–1729.
- Visconti, A., Le Roy, C.I., Rosa, F., Rossi, N., Martin, T.C., Mohney, R.P., et al., 2019. Interplay between the human gut microbiome and host metabolism. *Nat. Commun.* 10, 4505.
- Voith-Gaedert, L.E., Jonah, C., Momberg, D., Ngandu, B., Said-Mohamed, R., Oerther, D. B., et al., 2019. Assessment of environmental exposure factors on child diarrhea and systemic inflammation in the Eastern Cape. *Water Res.* 169, 115244.
- Wei, L., Rui, J., Si, H., X., Wu, J., W., S., et al., 2019. Investigating the toxicities of different functionalized polystyrene nanoplastics on *Daphnia magna*. *Ecotoxicol. Environ. Saf.* 180, 509–516.

- Xiao, F., Feng, L.-J., Sun, X.-D., Wang, Y., Wang, Z.-W., Zhu, F.-P., et al., 2022. Do polystyrene nanoplastics have similar effects on duckweed (*Lemna minor* L.) at environmentally relevant and observed-effect concentrations? Environ. Sci. Technol. 56, 4071–4079.
- Xu, M., Pokrovskii, M., Ding, Y., Yi, R., Au, C., Harrison, O.J., et al., 2018. c-MAF-dependent regulatory T cells mediate immunological tolerance to a gut pathobiont. Nature 554, 373–377.
- Xu, D., Ma, Y., Han, X., Chen, Y., 2021. Systematic toxicity evaluation of polystyrene nanoplastics on mice and molecular mechanism investigation about their internalization into Caco-2 cells. J. Hazard. Mater. 417, 126092.
- Yan, S., Tian, S., Meng, Z., Sun, W., Xu, N., Jia, M., et al., 2021. Synergistic effect of ZnO NPs and imidacloprid on liver injury in male ICR mice: increase the bioavailability of IMI by targeting the gut microbiota. Environ. Pollut. 294, 118676.
- Yan, Z., Liu, Y., Zhang, T., Zhang, F., Ren, H., Zhang, Y., 2022. Analysis of microplastics in human feces reveals a correlation between fecal microplastics and inflammatory bowel disease status. Environ. Sci. Technol. 56, 414–421.
- Yu, J., Chen, L., Gu, W., Liu, S., Wu, B., 2022. Heterogeneity effects of nanoplastics and lead on zebrafish intestinal cells identified by single-cell sequencing. Chemosphere 289, 133133.
- Zhang, J., Wang, L., Trasande, L., Kannan, K., 2021. Occurrence of polyethylene terephthalate and polycarbonate microplastics in infant and adult feces. Environ. Sci. Technol. Lett. 8, 989–994.
- Zhou, R., Wei, H., Sun, R., Zhang, J., Tian, Z., 2007. NKG2D recognition mediates Toll-like receptor 3 signaling-induced breakdown of epithelial homeostasis in the small intestines of mice. Proc. Natl. Acad. Sci. U. S. A. 104, 7512–7515.
- Zierer, J., Jackson, M.A., Kastenmüller, G., Mangino, M., Long, T., Telenti, A., et al., 2018. The fecal metabolome as a functional readout of the gut microbiome. Nat. Genet. 50, 790–795.